Radiative/Turbulent Transfer Interactions in Layer Clouds

HOWARD P. HANSON

Cooperative Institute for Research in Environmental Sciences, University of Colorado/NOAA, Boulder, CO 80309

(Manuscript received 4 June 1985; in final form 12 November 1986)

ABSTRACT

The differential absorption and emission of radiation with height inside clouds creates sources and sinks of buoyancy and thus can be an important factor in the turbulence-maintaining and dissipating processes of the clouds. This paper is concerned with the roles that solar and infrared radiation play in the turbulence budget of layer clouds, with primary emphasis on marine stratocumulus and inferential discussion of other layer cloud systems.

Physically realistic parameterizations of solar and infrared (IR) fluxes are used to show how the turbulence generation by cloud-top IR cooling can be more than offset by stabilization due to absorption of sunlight, and how the role of cloud-base IR warming depends crucially on the height of the cloud base. In the context of a mixed-layer model, these effects can be cast entirely in terms of the height of the layer's center of mass relative to the net heating and/or cooling due to the radiative transfer. Implications for the diurnal cycle and for a thin-cloud instability are discussed.

1. Introduction

The absorption and emission of radiation by clouds is a potentially important factor in their evolution and maintenance. Infrared (IR) cooling from the tops of stratocumulus clouds, for example, has long been known to contribute significantly to the clouds' turbulence generation (Lilly, 1968; Schubert, 1976). More recently, the role of the clouds' absorption of sunlight has begun to become appreciated as inducing a diurnal cycle in clouds (Oliver et al., 1978, Hanson and Gruber, 1982; Brill and Albrecht, 1982; Nicholls, 1984). This latter process is especially important due to its implications for cloud–climate interactions. Since low-level extended cloud cover acts primarily to decrease global heating (reflecting large amounts of sunlight while providing a minimal IR "greenhouse" effect), calculating *daytime* cloud cover in climate models is crucial. If the solar diurnal cycle is a significant factor in modulating the cloud cover's behavior, and it appears to be, the need for resolving it in climate models is indicated. The alternative is the development of a parameterization for daytime cloud cover based on daily averaged conditions. In either case, the interaction of radiative transfer processes and cloud dynamics becomes the central topic. This is the subject of the present paper.

As will be seen, the important factors in this interaction are not only the *amount* of energy absorbed and/or emitted by the cloud but also the *distribution* within the cloud of the resulting heating and cooling. In order to facilitate the use of simple cloud models in climate studies, parameterizations of the vertical profiles of solar and IR fluxes were derived by Hanson and Derr (1986; hereafter HD86). These parameterizations are based on exponential functions with cloud-edge flux values and decay scales derived from more detailed radiative transfer calculations. As exponential curves, the parameterized profiles are analytic and suitable for use in vertically integrated layer cloud models. This paper exploits this property to examine the implications for cloud turbulence generation of the solar and IR flux profiles. It will be seen that the solar diurnal cycle is quite important and, further, that the response of a stratocumulus cloud to the daytime heating could well be the separation of cloud and subcloud layers as discussed by Nicholls (1984). That this does not necessarily always happen will also be shown.

Section 2 contains an overview of the parameterization developed in HD86 and a presentation of the thermodynamic model used here, including a discussion of the turbulent entrainment closure problem and the present approach; basically, the issue is sidestepped with no loss of generality. Section 3 gives a discussion of results and section 4 is a summary.

2. Model

a. Radiative fluxes

As discussed in HD86, the matching of the parameterized flux profiles with the more detailed calculations preserves the important aspects of the flux distributions. The parameterized solar (F) and IR (G) net fluxes take the forms

$$F(z) = F_B - (F_B - F_C)\frac{\{1-\exp[-(z_B - z)/\lambda_{sol}]\}}{\{1-\exp[-(z_B - z_C)/\lambda_{sol}]\}} \quad (1)$$

and

$$G(z) = G_L \exp[-(z - z_C)/\lambda_L] + G_U \exp[-(z_B - z)/\lambda_U], \quad (2)$$

where z_B and z_C are the cloud top and base heights, respectively, F_B is the (net upward) cloud-top solar flux, F_C the cloud-base net solar flux and λ_{sol} the solar decay scale; G_U and G_L are the cloud top and base IR net fluxes, respectively, for very thick clouds (i.e., when λ_U and λ_L, the associated decay scales, are very small). The parameterization developed in HD86 yields values of F_B, F_C, G_U, G_L and $\lambda_{sol,U,L}$ given values of cloud liquid water content (LWC) and cloud optical properties. This is accomplished by constraining the cloud-edge values (i.e., cloud base and top fluxes) of the parameterized fluxes to match values obtained from the two-stream approximation and the emissivity method, for solar and IR radiation, respectively, and further by requiring the vertical integrals of the separate fluxes to match. The optical properties required are (solar) broadband single-scattering albedo and backscattering fraction and the IR emissivity. These values are obtained from Stephens (1978) and Stephens et al. (1984). Accordingly, the solar flux parameterization (1) is based on one absorbing band. More accuracy could be obtained—with concomittant increases in complexity and computer costs—by adding other bands; this would result in other exponential terms in (1). The development in HD86 hinged on the use of the two-stream approximation for the solar fluxes and the emissivity method for the IR fluxes, but other models would suffice. Rather than retain the relative complexity of these models, regressions were developed to give the decay scales $\lambda_{sol,U,L}$ solely as functions of the LWC. The final algorithm, summarized here as an Appendix, is quite straightforward and easily implemented even on microcomputers. Figures 1 give examples of the solar and IR flux profiles, and associated heating rates, for a 200 m thick cloud with the base at 400 m. The sensitivity of these profiles to cloud thickness, through its control of LWC, and the assumptions used in the derivation are discussed fully in HD86.

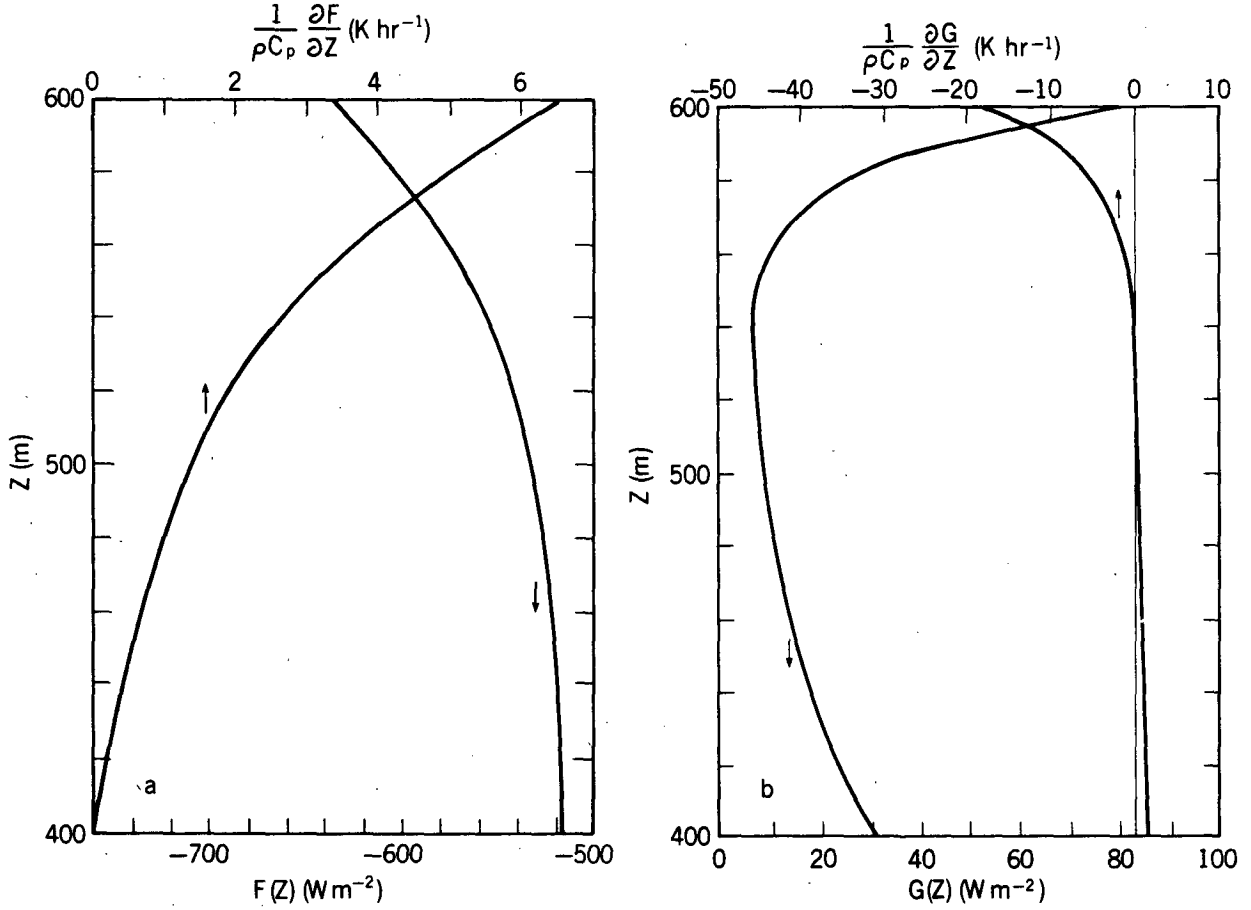

FIG. 1. (a) Solar and (b) IR fluxes (bottom scales) and heating rates (top scales), from Eqs. (1) and (2) for a 200 m cloud and quantities in Table 1.

b. Thermodynamics

Although the conceptual aspects of the radiative flux parameterization used here are widely applicable, it was implemented for clouds having liquid water mixing ratios that increase linearly with height. More specifically, it was derived for clouds in which total water mixing ratio (vapor plus liquid) is constant with height, that is, for a mixed-layer cloud. Mixed-layer models of the boundary layer oversimplify, to some extent, the physics of the layer, but they retain its most important features and, being vertically integrated, are attractive as boundary-layer modules for use in more comprehensive modeling studies. Their ability to predict countergradient heat fluxes and calculate the boundary-layer top in a Lagrangian sense is particularly useful. The most unrealistic constraint of such a model is the mixed-layer assumption itself, because it implies that fluxes of conservative quantities (such as total water mixing ratio) are linear with height. While quasi-linear flux profiles are commonly observed in the dry boundary layer over a heated surface and are present in laboratory simulations (e.g., Deardorff and Willis, 1985), as well as numerical calculations (Deardorff, 1980b) and observations (Brost et al., 1982) of the cloud-topped boundary layer, it is known that there are circumstances when linearity breaks down altogether (Deardorff, 1980a; Nicholls, 1984). Nonetheless, mixed layer models are useful as tools for studying the limiting case because of their extreme analytic simplicity. This property is used in the present paper to examine the interactions of radiation and turbulence in mixed layer models; qualitative inferences about other cases are also drawn.

Denoting total water mixing ratio by $r = q + l$ (where $q = q^*$—saturated—in cloud and $l = 0$ below cloud base) and defining the liquid static energy by $s = C_pT + gz - Ll$ (where C_p, g and L are the specific heat of air at constant pressure, gravitational acceleration and the latent heat of condensation, respectively, and T is the temperature) allows the thermodynamic budgets to be written without condensation/evaporation terms:

$$d\bar{r}/dt + \partial\overline{w'r'}/\partial z = 0 \tag{3}$$

and

$$d\bar{s}/dt + \partial\overline{w's'}/\partial z = -(\partial F/\partial z + \partial G/\partial z)/\rho. \tag{4}$$

Here, the substantial derivatives include storage and horizontal advection, ρ is an average air density and precipitation has been neglected. (Note that s is used here to denote *liquid* static energy, contrary to convention; this is to eliminate cumbersome subscripts in what follows.)

An alternative to liquid static energy s is the *moist* static energy h, the budget equation for which is the sum of (3) and (4). Using moist static energy as a dependent variable has the advantage that precipitation, if present, can be written in terms of fluxes that appear only in the total water budget, and the two budget equations, for total water and moist static energy, are perfectly symmetric, allowing them to be treated together as a vector. This provides the basis for Betts' (1982, 1983) Saturation Point Method (Hanson, 1984a). Although precipitation fluxes would appear in the liquid static energy budget, they are neglected here and liquid static energy is used because of its close relationship with potential temperature. Even for very thick clouds, the liquid water contribution Ll to s is of the order 1%, whereas the vapor contribution to h can be more than 10%. Further, the cloud-top inversion in terms of liquid static energy is always positive ($\Delta s \equiv s_U - s_M > 0$) while the sign of Δh can change. This implies that the cloud-top entrainment flux of s is always negative (while that for h can change sign) and thus simplifies the interpretation of the turbulent energetics considerably.

The mixed-layer structure for $\bar{r} = r_M$ and $\bar{s} = s_M$ requires that all terms in (3) and (4) be constant with height; this implies that

$$[\overline{w'r'}] \quad \text{and} \quad [\overline{w's'} + (F+G)/\rho]$$

must be linear with height. As a consequence, the exponential forms for F and G induce compensating exponential terms in $\overline{w's'}(z)$ within the cloud. This, in turn, affects the turbulence kinetic energy (TKE) budget and the entrainment closure for z_B in the model; i.e.,

$$\overline{w's'}(\tilde{z}) = [\overline{w's'_S} + (F_S + G_S)/\rho](1-\tilde{z}) + [\overline{w's'_B} + (F_B + G_B)/\rho]\tilde{z} - [F(\tilde{z}) + G(\tilde{z})]/\rho, \tag{5}$$

where $\tilde{z} \equiv z/z_B$. The surface and cloud-top turbulent fluxes can be obtained from the bulk drag and the entrainment flux formulas:

$$\overline{w's'_S} = v_S(C_pT_S - s_M) \tag{6a}$$

and

$$\overline{w's'_B} = -w_e(s_U - s_M). \tag{6b}$$

In (6a), v_S is the surface ventilation factor (the surface transfer coefficient times the 10-m wind speed), and in (6b), $w_e = dz_B/dt - \bar{w}_B$ is the entrainment rate—the subject of the turbulence closure—and $s_U(z_B)$ is the upper-air static energy profile. Similar formulas apply to the water fluxes. Any radiative flux divergence within the mean inversion is neglected here, albeit a subject of some recent controversy (Nieuwstadt and Businger, 1984), and the focus is the effects of heating and cooling *within* the cloud. To complete the thermodynamic model, the cloud base, z_C, can be diagnosed as the lifting condensation level for near-surface parcels.

c. Entrainment

Turbulence closures have been discussed recently by Randall (1984a); this paper concentrates on the turbulent buoyancy flux, which is a linear combination of $\overline{w's'}$ and the corresponding total water flux with dif-

ferent weighting in the cloud and subcloud layers. In the subcloud layer,

$$\overline{w'b'} = \overline{w's'} + \epsilon\delta L\overline{w'r'}, \tag{7a}$$

where b is a buoyancy variable (proportional to virtual potential temperature), $\delta = 0.608$ and $\epsilon = C_pT/L$ is a thermodynamic quasi-constant (Randall, 1980a); and

$$\overline{w'b'} = \beta\overline{w's'} + (\beta - \epsilon)L\overline{w'r'}, \tag{7b}$$

where β is proportional to the in-cloud temperature lapse rate (see HD86), in the cloud layer. Although details differ, all closures involve the vertical integral of this TKE source/sink mechanism in some form. In particular, the vertical integral is basic to the turbulent convective velocity scaling (e.g., Deardorff, 1980a):

$$w^{*3} = 2.5\frac{g}{C_p\theta}\int_0^{z_B}\overline{w'b'}dz \equiv 2.5\frac{gz_B}{C_p\theta}B, \tag{8a}$$

where θ is a reference temperature.

The liquid static energy contribution to the normalized buoyancy flux integral B can be written as the sum of five terms:

$$B_s \equiv S = S_S + S_B + S_{sol} + S_U + S_L. \tag{9}$$

The turbulent convective velocity scale is then

$$w^{*3} = 2.5\frac{gz_B}{C_p\theta}(S + R), \tag{8b}$$

where R is the total water contribution analogous to (9). Using $\zeta \equiv z_C/z_B$, the turbulent surface and entrainment flux contributions in (9) are

$$S_S = 0.5\overline{w's'_S}[(2-\zeta)\zeta + \beta(1-\zeta)^2], \tag{10a}$$

$$S_B = 0.5\overline{w's'_B}[\zeta^2 + \beta(1-\zeta^2)]. \tag{10b}$$

The total water contribution, R, to B consists of terms analogous to (10a) and (10b) with the first terms multiplied by $\epsilon\delta$, and β replaced by $(\beta - \epsilon)$.

The solar contribution to S is

$$S_{sol} = (F_B - F_C)/\rho\Lambda_{sol}(\lambda_{sol}), \tag{10c}$$

and the IR contributions from the cloud top and base are

$$S_U = G_U/\rho\Lambda_U(\lambda_U), \tag{10d}$$

$$S_L = G_L/\rho\Lambda_L(\lambda_L). \tag{10e}$$

The functions Λ, which describe the efficiency of the radiative transfer in modifying the turbulence (see the following), are

$$2\Lambda_{sol}(\lambda) = \zeta^2 + \beta(1-\zeta) \times \{2/[1-\exp(-1/\hat{\lambda})] - 2\hat{\lambda} + \zeta - 1\}, \tag{11a}$$

$$2\Lambda_U(\lambda) = \zeta^2[1-\exp(-1/\hat{\lambda})] + \beta(1-\zeta) \times \{1 + \exp(-1/\hat{\lambda}) - (2\hat{\lambda} - \zeta)[1-\exp(-1/\hat{\lambda})]\}, \tag{11b}$$

$$2\Lambda_L(\lambda) = -\zeta^2[1-\exp(-1/\hat{\lambda})] + \beta(1-\zeta) \times \{1 + \exp(-1/\hat{\lambda}) - (2\hat{\lambda} + \zeta)[1-\exp(-1/\hat{\lambda})]\}, \tag{11c}$$

where the decay scales are normalized by the cloud thickness: $\hat{\lambda} \equiv \lambda/(z_B - z_C)$.

The five liquid static energy contributions to the turbulence scaling velocity therefore depend on relevant flux values and nondimensional functions. The nondimensional functions for the turbulent fluxes, at the surface and the cloud top, depend only on the relative thicknesses of the cloud and subcloud layers via the parameter ζ. The nondimensional functions Λ for the radiative flux contributions to w^* also depend on the decay scales and the actual value of the cloud thickness, through the $\hat{\lambda}$'s. In HD86 it was shown that the cloud LWC in a mixed layer model is proportional to the square of the cloud thickness; further, the decay scales were parameterized as direct functions of LWC. This additional dependence of the radiative fluxes over the turbulent fluxes has important implications for the overall turbulence budget, as shown in section 3.

In order to calculate w_e, further constraints must be placed on the buoyancy-flux integral B, as discussed by Randall (1984a). In the clear mixed layer, the buoyancy flux at the top of the layer is usually taken to be a constant fraction $(-A)$ of the surface flux; the commonly used value of $A = 0.2$ is the origin of the factor 2.5 in (8) [$2.5 = 2/(1 - A)$]. In the cloud-topped mixed layer, the two main closures for w_e equate either (fractions of) the positive and negative S's and R's (Stage and Businger, 1981a,b) or (fractions of) the positive and negative areas under the $\overline{w'b'}$ curve (Randall, 1980b). Randall (1984a) classifies these two approaches as "process" partitioning and "Eulerian" partitioning, respectively. It is clear from (5) that the radiative flux formulation used here would make Eulerian partitioning very difficult to implement, while implementation of process partitioning would be straightforward. By examining the roles of solar and IR radiation in changing w^*, via (8) and (9), it is possible to infer their effects on mixed-layer turbulence and entrainment without choosing a particular closure method.

3. Results

By examining the turbulent energetics of the layer in terms of the scaling velocity w^*, then, it is possible to avoid the issue of the entrainment closure technique. All entrainment closures, regardless of details, retain the physically appealing property that the entrainment rate w_e varies in some direct relationship with w^*. The dependence of w^* on B allows the effects of the radiative fluxes on entrainment to be deduced through the behavior of the nondimensional functions Λ and the multiplying fluxes in Eqs. (10c–e).

It is first instructive to examine the corresponding functions, appearing in (10a) and (10b), that multiply the turbulent fluxes at the surface and cloud top, i.e.,

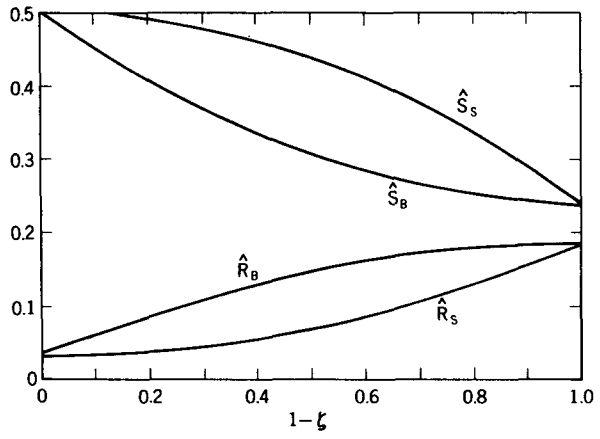

FIG. 2. Nondimensional efficiencies of surface and cloud-top turbulent fluxes at generating turbulence vs relative cloud layer depth.

$\hat{S}_{B,S} \equiv S_{B,S}/(\overline{w's'_{B,S}})$. Physically, these represent the ratios of the layer-averaged buoyancy flux to the cloud-top (or surface) liquid static energy flux in the absence of other processes. This interpretation also applies to the water vapor and radiative fluxes. Thus, each of these ratios (and the functions Λ) can be viewed as an efficiency factor for a specific process relative to w^*. The ratios are shown in Fig. 2 as functions of the relative depth of the cloud layer $1 - \zeta$. For $1 - \zeta = 0$, there is no saturation and the layer is a *dry* mixed layer so the water contributions are limited to the (small) vapor correction to the buoyancy flux. For $1 - \zeta = 1$, the cloud base $z_C = 0$ and the layer is marginally a fog layer (with $l = 0$ just at the surface), so that the water contributions to $\hat{R}_{B,S} \equiv R_{B,S}/(L\overline{w'r'_{B,S}})$ become more important and the analogous liquid static energy contributions less so. This variability is due to the role of condensation, evaporation and liquid water loading in the cloud layer. Marine stratocumulus layers typically occur with very small Bowen ratios, in which case R_S can be larger than S_S despite the relationship shown in Fig. 2. Cloud-top entrainment fluxes of r are always positive (dry air is entrained downward), and so R_B is positive, but, since $\Delta s > 0$, $\overline{w's'_B} < 0$ and S_B is always negative. Cloud-top entrainment instability (Deardorff, 1980a; Randall, 1980a) occurs when Δs is small and Δr is large (and negative) and (7b) at the cloud top becomes *positive*. Although this instability will increase w^* (and w_e), it will not necessarily lead to a breakup of a solid cloud deck (Hanson, 1984b).

TABLE 1. Specified quantities.

Quantity	Symbol	Value
Cloud base height	z_C	400 m
Cloud base temperature	T_C	284 K
In-cloud temperature gradient	$-\beta g/C_p$	$-0.48g/C_p$ K m^{-1}
Upward cloud-base IR flux	$G_C\uparrow$	385 W m^{-2}
Downward cloud-top IR flux	$G_B\downarrow$	$(305 - 0.03z_B)$ W m^{-2}
Downward cloud-top solar flux	$F_B\downarrow/\mu_0$	1210 W m^{-2}

Due to the dependence of the decay scales λ on the cloud LWC, it is necessary to introduce physical conditions to evaluate the Λ's. Table 1 gives the values used here, which are typical for marine stratocumulus. Figure 3 shows the behavior of $\Lambda_{sol,U,L}$ as a function of cloud thickness $\Delta z \equiv z_B - z_C$. (Although $\Delta z \to 0$ introduces apparent singularities into the $\hat{\lambda}$'s, their dependence on the LWC and the limiting process allows analytic evaluation of the Λ's at $\Delta z = 0$.) The odd "hump" of Λ_L at $\Delta z \sim 250$ m is due to the behavior of λ_L (see HD86).

Physical interpretation of the curves in Fig. 3 is straightforward and can be made in terms of the position of the heating and cooling relative to the mixed layer's center of mass (CM). The solar contribution S_{sol} is, of course, associated with heating and, since $\Delta F \equiv F_B - F_C < 0$ always, $S_{sol} < 0$. For very thin clouds, with $z_C = 400$ m, the CM is in the subcloud layer and the heating is above, in the cloud, so the warming impedes turbulence generation. As the clouds become thicker, the effective position of the solar heating rises somewhat more rapidly than the CM and Λ_{sol} decreases but remains positive. Although there is heating within the cloud, which can contribute positively to S_{sol}, the net vertically integrated solar contribution is always negative.

The efficiency of the cloud-base IR fluxes at modifying the turbulence (through Λ_L) exhibits the opposite behavior. For thin clouds, Λ_L is negative, reflecting heating at the top of the mixed layer (since $z_C = 400$ m). As the cloud becomes thicker, the cloud-base heating (see Fig. 1b) becomes nearer the CM; in this example, the crossover occurs off scale at $\Delta z \sim 680$ m, and the cloud-base heating begins to generate turbulence rather than impede it.

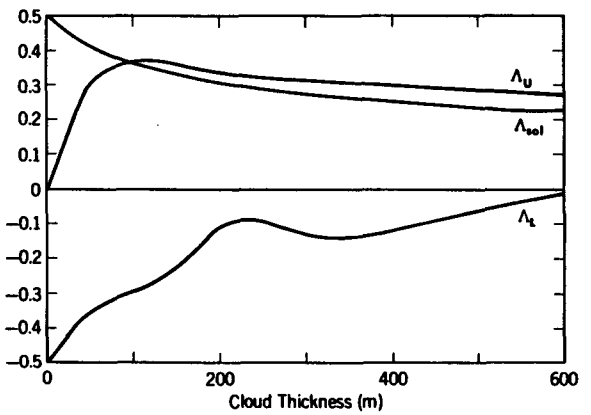

FIG. 3. Radiative flux efficiencies at generating turbulence as function of cloud thickness for $z_C = 400$ m.

The efficiency of the cloud-top IR cooling Λ_U is somewhat more complicated. For very thin clouds, the decay scale λ_U is very large and the cooling is therefore small, so the net turbulence generation vanishes at $\Delta z = 0$. As the clouds become thicker, λ_U decreases rapidly and the cooling not only becomes stronger but also becomes more concentrated near the top of the cloud layer; thus, Λ_U increases rapidly. At the same time, however, the layer's overall mass is increasing and, near $\Delta z = 100$ m in Fig. 3, the rapid increase of Λ_U is overcome by this factor. Subsequent decreases in λ_U are mitigated by the layer's increasing mass and Λ_U decreases slowly for thicker clouds.

Since all radiative heating is due to clouds (in the implementation of the radiative parameterization discussed here), it is to be expected that $S_{sol,U,L}$ should vanish as $\Delta z \to 0$. The upper IR contribution does indeed vanish, since Λ_U vanishes. It turns out that the solar and lower IR contributions also vanish, because the multiplying fluxes ΔF and G_L vanish, as shown in Fig. 4. (The IR parameterization is formulated such that, for the zero-cloud-thickness limit, $G_U = G_C\uparrow - G_B\downarrow$.) In Fig. 4, the minimum in G_U is due to the behavior is λ_L and the maximum of G_L is due to a combination of the rapid decrease of λ_U and the *increase* of λ_L in the thin cloud regime (see HD86).

Figure 5 shows the total contributions of the radiative fluxes to the buoyancy flux integral. The net effect of the radiative fluxes is turbulence generation for clouds thinner than about 110 m. For thicker clouds, the solar heating stabilizes the layer, with some assistance from the cloud-base IR heating, and the fluxes impede the turbulence. The crossover point clearly depends strongly on the magnitude of ΔF, which, in the parameterization, is derived from the bulk cloud absorption parameterization of Stephens et al. (1984). As shown in HD86, this absorption scheme consistently predicts values somewhat too high compared to observations;

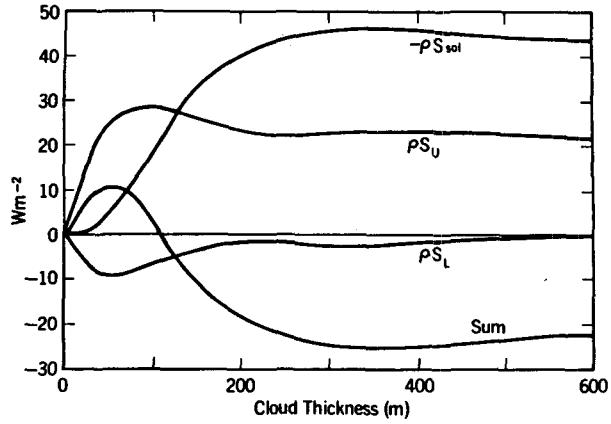

FIG. 5. Radiative contributions to the virtual static energy flux integral as a function of cloud thickness for $z_C = 400$ m.

reducing the values of ΔF accordingly would put the zero-crossing of the sum in Fig. 5 at $\Delta z \sim 200$ m.

Furthermore, the solar fluxes used here are all calculated for a solar zenith angle of unity. Nonequatorial latitudes at times other than noon, or upper-level clouds, would further decrease the ΔF and increase the zero-crossing in Fig. 5. This implies, clearly, a strong effect of the diurnal cycle on the mixed layer's turbulence budget. Unless the surface fluxes are strong enough to overcome the stabilization due to solar heating, the turbulence cannot be maintained throughout the layer during daytime.

It is this phenomenon that has lead Nicholls (1984) to suggest that the stratocumulus-topped mixed layer may, effectively, separate during midday. When decoupled from the subcloud layer, the effect of radiative fluxes in the cloud layer change radically. Figure 6 shows the radiative-flux contributions to the buoyancy flux integral for the case $z_C = 0$ (while retaining the other values in Table 1). Although this refers to a fog layer, the algebra of Eqs. (10c–e) is such that it also

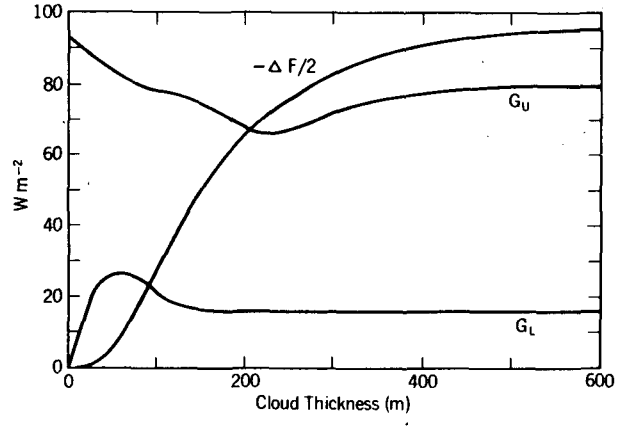

FIG. 4. Radiative fluxes forcing (or damping) turbulence vs cloud thickness. The case shown applies to $z_C = 400$ m, but these values are relatively independent of the cloud-base height.

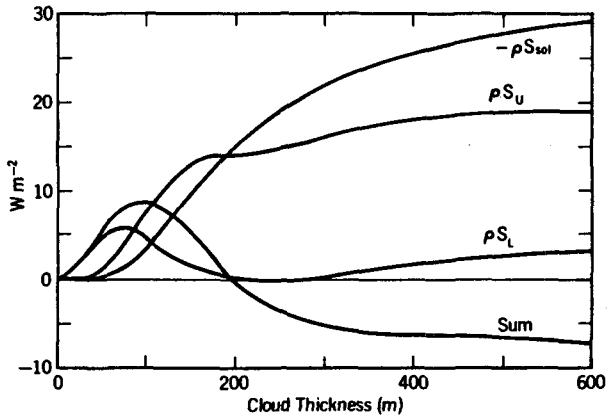

FIG. 6. As in Fig. 5 for $z_C = 0$.

applies to an elevated cloud layer for which the mixing extends only to cloud base. In this case, the sum of the radiative contributions remains positive until $\Delta z \sim 200$ m; reduction of the solar heating as discussed previously would further increase the zero-crossing to ~400 m. The change is entirely due to changes in the Λ's, as shown in Fig. 7. Since the CM of the "mixed layer" is now in midcloud, the cloud base IR heating always generates turbulence, although at very small levels in this case (Fig. 6), because the upward flux into the cloud nearly balances the downward IR flux from cloud base. The overall values of $\Lambda_{sol,U}$ are lower because of the reduced role of the liquid static energy fluxes in the cloud (through the factor β). Since there is no subcloud layer mass to be stirred, the cloud-top IR cooling is relatively more effective than the solar heating, because it is more concentrated near the layer's top. The net effect of these changes is to make it possible to maintain a well-mixed cloud in the face of substantial solar heating. However, the *cause* of the separation of the two layers cannot be explained in this fashion. This discussion concerns the *effect* on the turbulence of the separation. In particular, the specific mechanisms at work in these circumstances require more research, for which a mixed-layer model is inadequate. It should be noted that not all stratocumulus-topped mixed layers will always separate. If the cloud is sufficiently thin, if the surface fluxes are sufficiently strong, and/or if the solar heating is sufficiently weak (due, for example to midlevel clouds), the turbulence can be maintained throughout the layer all day.

A final result of interest concerns the increase, for thin clouds, of S_U and the sums shown in Figs. 5 and 6. Recently, Randall and Suarez (1984) presented results from numerical calculations in which cyclic forcing (in their case, changing the large-scale divergence) of a stratocumulus layer resulted in a hysteresis effect: beginning with a clear mixed layer, decreasing the divergence caused the layer to deepen; when it reached the condensation level, the formation of a cloud, and initiation of cloud-top cooling, caused a rapid growth of the depth of the layer. In contrast, on *increasing* the divergence, the cloud persisted for much larger divergences than when the cloud first formed. In addition, as the divergence increased, the cloud thinned rapidly after a critical thickness was reached, and, in the range of thicknesses lower than this critical value, no equilibrium was possible even for constant forcing.

These effects, in Randall and Suarez' (1984) model, were due to a cloud-top IR cooling formulation that crudely simulated the effect of nonblack clouds for small Δz. It is, of course, also present in the method used in this paper, and is the reason for the positive slope of S_U for thin clouds in Figs. 5 and 6. This *thin-cloud instability* is caused by a positive correlation of the efficiency of cloud-top IR cooling at generating turbulence and deeper clouds. As pointed out by Randall (1984b), stronger entrainment does not always cause clouds to become thicker; therefore, the instability applies only to cases in which the cloud is supplied with sufficient moisture, either from below or by horizontal advection, so that it can compensate for the increased entrainment of dry air from above and become thicker. Note that while the instability persists for only a limited depth range in the case of an elevated cloud layer (Fig. 5), it persists for all values of the depth of a fog layer (Fig. 6). This latter result also applies to elevated, isolated cloud layers, given a moisture source sufficient to overcome the drying due to entrainment. An analogous positive feedback occurs for thicker clouds with respect to the cloud-base IR contribution S_L. Although small in this case, due to the imposed proximity of the cloud base to the surface and consequently small G_L, it is potentially significant for elevated, isolated cloud layers where the cloud-base temperature is much less than the effective radiating temperature below the cloud. In contrast, since $\Delta F < 0$, the solar contribution always constitutes a negative feedback.

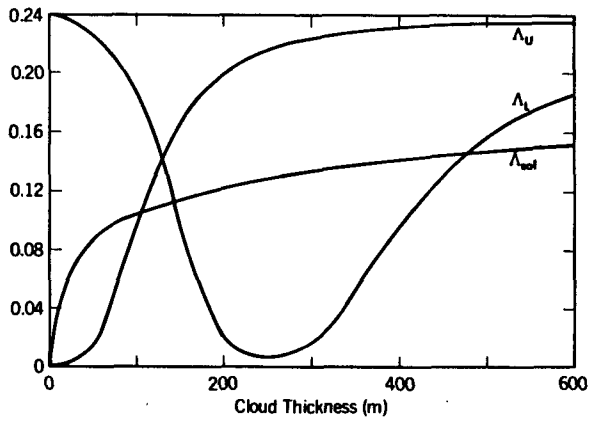

FIG. 7. As in Fig. 3 for $z_C = 0$.

4. Conclusion

Although the interactions between radiation and extended cloud cover have been included in studies of climate and cloud dynamics for some time, in most cases the radiative heating and cooling have been only crudely represented. The analyses in this paper have been an attempt to remedy this situation with the simplest possible realistic model. In Hanson and Derr (1986), parameterizations for solar and IR net fluxes within idealized clouds were developed. These take the form of exponential functions of height, with the decay scales parameterized as functions of cloud liquid water content. As exponential functions, the fluxes are easily included in (vertically integrated) mixed layer models, and, in particular, their effects on the mixed-layer turbulence energy can be examined analytically. Because the sum of radiative and turbulent fluxes in a mixed

layer model must be linear, the radiative fluxes induce compensating exponential terms in the model heat flux profile, which in turn affects the buoyancy flux profile. The latter governs the turbulence scaling velocity and, with further assumptions, the entrainment closure.

Since solar heating occurs above the mixed layer's center of mass, it always tends to stabilize the layer and, through its influence of the buoyancy flux, impede turbulence generation. The degree to which this occurs depends strongly on the relative depths of the cloud and subcloud layers. For deeper subcloud layers, the solar heating is relatively more efficient at impeding turbulence generation due to the layer's lower center of mass. As the cloud layer becomes thicker, the center of the heating rises and continues to impede turbulence generation. This has clear implications for a diurnal cycle: cloud-topped mixed layers established at night will become subject to large readjustments during the day. One such adjustment could be the separation of the cloud and subcloud layers, as discussed by Nicholls (1984). In this case, the efficiency of the solar heating at impeding the turbulence is greatly diminished. The mechanisms of this separation are yet to be elucidated.

Cloud-base IR warming plays a changing role in the mixed layer's turbulent energetics that is dependent on the position of the cloud base relative to the layer's center of mass. If the subcloud layer is shallow enough, the warming is below the center of mass and generates turbulence. In such a case, the turbulence generation will be small for a surface-linked mixed layer. On the other hand, it could be large and even dominant for elevated, isolated clouds such as mid- and upper-level stratus and cirrus. The current radiative parameterization is not formulated specifically for these clouds, but this qualitative conclusion is likely to apply.

The role of cloud-top IR cooling is always to generate turbulence, and its efficiency also depends strongly on the subcloud and cloud layers' thicknesses. A particularly interesting aspect of this behavior is the implication of a thin cloud instability such as that revealed by the numerical calculations reported by Randall and Suarez (1984). If sufficient moisture is available, increases in cloud entrainment can produce thicker clouds, which increase the IR cooling's efficiency at generating turbulence and further increasing entrainment; the reverse scenario also applies. This positive feedback is not limited by cloud thickness in an isolated cloud layer such as a fog layer or an elevated, separated cloud layer. The strength of the feedback will depend strongly on the specific entrainment closure used in the mixed-layer model. Studies, now in progress, are comparing the response of various closures to the radiative flux parameterization used here.

Acknowledgments. This paper is a result of research supported by National Science Foundation through Grants ATM 82-09115 and OCE 85-00860.

APPENDIX

Radiative Flux Parameterization

This appendix presents the radiative flux parameterization including the regression formulas for the decay scales developed in HD86. In that paper, the emphasis was on describing the shapes of radiative flux profiles within simple clouds using exponential functions. Accordingly, the parameterization relies on values of several quantities as external conditions. These include z_B, z_C, W, T_B, T_C, all of which are defined in the text; the downward solar flux at the top of the boundary layer and its zenith angle cosine, $F_B\downarrow$, μ_0, respectively; the upward and downward IR fluxes at the cloud base and top, $G_C\uparrow$, $G_B\downarrow$, respectively; and the emissivity parameters $\alpha\uparrow$ (=0.13), and $\alpha\downarrow$ (=0.158). For the solar flux calculation, it is first necessary to use the parameterization of Stephens et al. (1984) (or some other suitable method) to find R_{net} and Ac_{net}, the net albedo and absorptance of the cloud, respectively. Then

$$\lambda_{sol} = 15.0W^{0.335},$$

$$F_B = -(1-R_{net})F_B\downarrow,$$

$$F_C = F_B + Ac_{net}F_B\downarrow,$$

$$F(z) = F_B - (F_B - F_C)\frac{\{1-\exp[-(z_B-z)/\lambda_{sol}]\}}{\{1-\exp[-(z_B-z_C)/\lambda_{sol}]\}}.$$

This is Eq. (1) of the text. For the IR flux parameterization,

$$\lambda_U = 140.0W^{-0.56},$$

$$\lambda_L = 70.W/(W - W^{1/2} + 2.67),$$

$$B_B \equiv \sigma T_B^4,$$

$$B_C \equiv \sigma T_C^4,$$

$$\eta\uparrow,\downarrow \equiv \alpha\uparrow,\downarrow W,$$

$$\tilde{G}_0 \equiv G_C\uparrow - B_C + (B_C - G_B\downarrow)\exp(-\eta\downarrow),$$

$$\tilde{G}_1 \equiv (G_C\uparrow + B_B - 2B_C)\exp(-\eta\uparrow) + B_B - G_B\downarrow,$$

$$1/\lambda_N \equiv 1/\lambda_U + 1/\lambda_L,$$

$$\hat{D} \equiv 1 - \exp(-(z_B - z_C)/\lambda_N),$$

$$G_U = \{\tilde{G}_1 - \tilde{G}_0\exp[-(z_B - z_C)/\lambda_L]\}/\hat{D},$$

$$G_L = \{\tilde{G}_0 - \tilde{G}_1\exp[-(z_B - z_C)/\lambda_U]\}/\hat{D},$$

$$G(z) = G_L\exp[-(z - z_C)/\lambda_L] + G_U\exp[-(z_B - z)/\lambda_U].$$

This is Eq. 2 of the text.

REFERENCES

Betts, A. K., 1982: Cloud thermodynamic models in saturation point coordinates. *J. Atmos. Sci.*, **39**, 2182–2191.

——, 1983: Thermodynamics of mixed stratocumulus layers: Saturation point budgets. *J. Atmos. Sci.*, **40**, 2655–2670.

Brill, K., and B. Albrecht, 1982: Diurnal variation of the trade-wind boundary layer. *Mon. Wea. Rev.*, **110,** 601–613.

Brost, R. A., J. C. Wyngaard and D. H. Lenschow, 1982b: Marine stratocumulus layers. Part II: Turbulence budgets. *J. Atmos. Sci.*, **39,** 818–836.

Deardorff, J. W., 1980a: Cloud top entrainment instability. *J. Atmos. Sci.*, **37,** 131–147.

——, 1980b: Stratocumulus-capped mixed layers derived from a three-dimensional model. *Bound.-Layer Meteor.*, **18,** 495–527.

——, and G. E. Willis, 1985: Further results from a laboratory model of the convective planetary boundary layer. *Bound.-Layer Meteor.*, **32,** 205–236.

Hanson, H. P., 1984a: On mixed-layer modeling of the stratocumulus-topped marine boundary layer. *J. Atmos. Sci.*, **41,** 1226–1234.

——, 1984b: Stratocumulus instability reconsidered: a search for physical mechanisms. *Tellus*, **36,** 355–368.

——, and P. L. Gruber, 1982: Effect of marine stratocumulus clouds on the ocean-surface heat budget. *J. Atmos. Sci.*, **39,** 897–908.

——, and V. E. Derr, 1986: Parameterization of radiative flux profiles in layer clouds. Submitted to *J. Climate Appl. Meteor.*

Lilly, D. K., 1968: Models of cloud-topped mixed layers under a strong inversion. *Quart. J. Roy. Meteor. Soc.*, **94,** 292–309.

Nicholls, S., 1984: The dynamics of stratocumulus: aircraft observations and comparisons with a mixed layer model. *Quart. J. Roy. Meteor. Soc.*, **110,** 783–820.

Nieuwstadt, F. T. M., and J. A. Businger, 1984: Radiative cooling near the top of a cloudy mixed layer. *Quart. J. Roy. Meteor. Soc.*, **110,** 1073–1078.

Oliver, D. A., W. S. Lewellen and G. G. Williamson, 1978: The interaction between turbulent and radiative transport in the development of fog and low-level stratus. *J. Atmos. Sci.*, **35,** 301–316.

Randall, D. A., 1980a: Conditional stability of the first kind upside-down. *J. Atmos. Sci.*, **37,** 125–130.

——, 1980b: Entrainment into a stratocumulus layer with distributed radiative cooling. *J. Atmos. Sci.*, **37,** 148–159.

——, 1984a: Buoyant production and consumption of turbulence kinetic energy in cloud-topped mixed layers. *J. Atmos. Sci.*, **41,** 402–413.

——, 1984b: Stratocumulus cloud deepening through entrainment. *Tellus*, **36A,** 446–457.

——, and M. J. Suarez, 1984: On the dynamics of stratocumulus formation and dissipation. *J. Atmos. Sci.*, **41,** 3052–3057.

Schubert, W. H., 1976: Experiments with Lilly's cloud-topped mixed layer model. *J. Atmos. Sci.*, **33,** 436–446.

Stage, S. A., and J. A. Businger, 1981a: A model for entrainment into a cloud-topped marine boundary layer. Part I: Model description and application to a cold-air outbreak episode. *J. Atmos. Sci.*, **38,** 2213–2229.

——, and ——, 1981b: A model for entrainment into a cloud-topped marine boundary layer. Part II: Discussion of model behavior and comparison with other models. *J. Atmos. Sci.*, **38,** 2230–2242.

Stephens, G. A., 1978: Radiation profiles in extended water clouds. II: Parameterization. *J. Atmos. Sci.*, **35,** 2123–2132.

——, S. Ackerman and E. A. Smith, 1984: A shortwave parameterization revised to improve cloud absorption. *J. Atmos. Sci.*, **41,** 687–690.